Unsupervised Manifold Clustering of Topological Phononics

Yang Long, Jie Ren,* and Hong Chen
Center for Phononics and Thermal Energy Science, China-EU Joint Center for Nanophononics, Shanghai Key Laboratory of Special Artificial Microstructure Materials and Technology, School of Physics Sciences and Engineering, Tongji University, Shanghai 200092, China

(Received 1 August 2019; accepted 13 April 2020; published 6 May 2020)

Classification of topological phononics is challenging due to the lack of universal topological invariants and the randomness of structure patterns. Here, we show the unsupervised manifold learning for clustering topological phononics without any *a priori* knowledge, neither topological invariants nor supervised trainings, even when systems are imperfect or disordered. This is achieved by exploiting the real-space projection operator about finite phononic lattices to describe the correlation between oscillators. We exemplify the efficient unsupervised manifold clustering in typical phononic systems, including a one-dimensional Su-Schrieffer-Heeger–type phononic chain with random couplings, amorphous phononic topological insulators, higher-order phononic topological states, and a non-Hermitian phononic chain with random dissipations. The results would inspire more efforts on applications of unsupervised machine learning for topological phononic devices and beyond.

DOI: 10.1103/PhysRevLett.124.185501

Topological phononics unveil complex mechanisms behind unconventional phononic wave phenomena [1–7], which lead to the backscattering immune phononic transport modes [8–12] and would be a promising route to the future robust on-chip communication devices [2,13–17]. To characterize nontrivial phononic topological properties, the key fundamental physical concept is the topological invariant, which is responsible for classifying the topological classes. However, there is *no* universal topological invariant for all topological phononic systems. Furthermore, it is even difficult to properly define them when considering many aspects, such as symmetry conditions [17], geometry features [11], and material dispersive responses [12]. Yet, no matter whether topological invariants are well defined or not, topological properties of phononic states are essentially embedded in the global structure features. So far, most of topological invariants are defined based on the Bloch-momentum space of the perfect periodic structure [5,15,18,19]. However, these momentum-based approaches will have inevitable shortages or inapplicability when handling phononic models like the spatial randomness of mechanical parameters, non-Hermitian features, or amorphous structures. Therefore, finding a general way to explore the topological properties based on real space without defining topological invariants *ad hoc* will be significant but also challenging for the future development of topological phononics and beyond.

Machine learning has shown the power on condensed matters, quantum domains, and topological physics [20–24], e.g., the phase learning of quantum many-body systems [25–29], inverse design of topological optics [30,31], and optimization of metamaterial devices [32–34]. However, most of these research works focus on supervised learning, which cannot capture the sample features without *a priori* knowledge and needs extensive samples with well-defined labels. Recently, unsupervised learning, which can find potential principles behind raw datasets without labels, has been attracting much attention about its ability on phase detections and classifications in spin systems [35–37], particle explorations in high energy physics [38,39], and efficient material discoveries [40]. Therefore, unsupervised machine learning would be the meaningful and powerful way to detect and classify topological properties from abundant phononic structures without any *a priori* knowledge about the topological mechanism.

In this Letter, we demonstrate the unsupervised manifold clustering of topological phononics based on similarities of dynamic properties in real space. The real-space dynamic properties of phononic system are represented by its projection operator $\hat{P}$, which reflects the responses and correlations between oscillators and thus contains the necessary information about the topological properties [41–44]. We first show manifold learning can unsupervisedly learn the features about the finite one-dimensional (1D) Su-Schrieffer-Heeger (SSH) chain efficiently and classify the topological classes due to nonlinear dimensional reduction [45,46]. Then, based on the real-space descriptions, we successfully demonstrate the unsupervised clustering of several topological phononics cases: (1) disordered phononic SSH chain with random couplings, (2) amorphous phononic systems with nonzero local Chern number, (3) higher-order phononic models, and (4) non-Hermitian phononic chain with random dissipation terms. These phononic systems are mapped into points of

the manifold space with reduced dimensions based on real-space features and are thus conveniently classified into different groups associated with different topological properties.

Let us introduce the real-space descriptors of phononic systems. The dynamic equations of a phononic system can be written as $\hat{H}|\psi_l\rangle = \Omega_l|\psi_l\rangle$, where ψ_l means the lth mode eigenstate of $\hat{H}$ with the frequency ω_l ($\Omega_l = \omega_l^2$), $l = 1, \ldots, L$ with L as the system size. The time-reversal counterpart will be $\hat{H}^\dagger|\varphi_l\rangle = \Omega_l^*|\varphi_l\rangle$. Therefore, the projection operator $\hat{P}$ of cutoff frequency ω_c is introduced as [41–44,47,48]

$$\hat{P} = \sum_{\omega_l \le \omega_c} |\psi_l\rangle\langle\varphi_l|. \tag{1}$$

When the system is Hermitian $\hat{H} = \hat{H}^\dagger$, $\langle\varphi_l| = \langle\psi_l|$. $\hat{P}$ describes the responses and correlations between the phononic oscillators, $P_{ij} = \langle x_j|\hat{P}|x_i\rangle$, playing the role of Green's function. Using $\hat{P}_n$ to denote the $L \times L$ matrix $\hat{P}$ of the nth sample ($n \in N$) in a set of N different realizations of the Hamiltonian parameters, we introduce a Gaussian kernel with controlled variance ε to define the similarity between samples n and n'

$$K_\varepsilon(n, n') = \exp\left(-\frac{||\hat{P}_n - \hat{P}_{n'}||^2}{2\varepsilon L^2}\right), \tag{2}$$

where $||\cdot||$ is the taxicab $\mathbb{L}^1$-norm distance, $||A|| = \sum_i \sum_j |A_{ij}|$. We can see that Eq. (2) reflects the similarity by calculating the projection operator between two phononic samples n and n' such that $K_\varepsilon(n, n') \approx 1$ when $\hat{P}_n$ can transform into $\hat{P}_{n'}$ with small deformation. If considering the topological invariant v that is a function of $\hat{P}$ and $v(\hat{P} + \Delta\hat{P}) \approx v(\hat{P}) + \{[\partial v(\hat{P})]/\partial\hat{P}\}\Delta\hat{P}$, the difference between different $\hat{P}$ will be responsible for classifying the topological properties $v(\hat{P})$, namely, $|v(\hat{P}_n) - v(\hat{P}_{n'})| \propto ||\hat{P}_n - \hat{P}_{n'}||$. Different topological classes with distinct invariants will have small similarity K_ε.

We exploit the typical manifold learning algorithm based on probabilistic transition process: the diffusion map, which has been widely used and developed in data science [49,50]. The diffusion process is defined by the local probability transition matrix $T_{n,n'} = (1/Z_n)K_\varepsilon(n, n')$, where $Z_n = \sum_{n'=1}^N K_\varepsilon(n, n')$ is the normalization term guaranteeing the probability conservation $\sum_{n'} T_{n,n'} = 1$. The global diffusion distance between sample n and n' after t steps can be described by $d_t(n, n') \equiv \sum_{n''}(1/Z_{n''})|T^t_{n,n''} - T^t_{n',n''}|^2 = \sum_{j=1}^{N-1} \lambda_j^{2t}|(\phi_j)_n - (\phi_j)_{n'}|^2 \ge 0$, where the ϕ_j are the jth right eigenvectors of $\hat{T}$, $\hat{T}\phi_j = \lambda_j\phi_j$, with the ordered eigenvalues $\lambda_{N-1} \le \cdots \le \lambda_2 \le \lambda_1 \le 1 = \lambda_0$. The $j = 0$ diffusion mode does not contribute since it is a constant vector. It is clear that after long time diffusion $t \to \infty$, the first few components ϕ_j with largest eigenvalues λ_j will dominate, which means that we only need a few components ϕ_j to represent the samples well so as to reduce the dimension. In particular, the number of the top-ranked largest eigenvalues λ_j could determine the number of topological clusters without *a priori* knowledge [37,49,50]. In addition to the diffusion map demonstrated here, other alternative manifold learning algorithms, i.e., spectral clustering, can be also used to obtain similar results. The main points are the real-space descriptor (1) and the similarity (2) to properly describe the sample distances.

Topological phononics with random couplings.—We use the finite 1D SSH phononic chain model [2] to demonstrate the unsupervised clustering of topological phononics in Fig. 1(a). The dynamic equation can be written as

$$\begin{aligned} m\frac{\partial^2}{\partial t^2}a_i &= -\kappa_1(a_i - b_{i-1}) + \kappa_2(b_i - a_i), \\ m\frac{\partial^2}{\partial t^2}b_i &= -\kappa_2(b_i - a_i) + \kappa_1(a_{i+1} - b_i), \end{aligned} \tag{3}$$

where a_i and b_i are the displacements of two atoms in the ith unit cell from their equilibrium positions, the elastic constants $\kappa_1 = \kappa_0\delta$, $\kappa_2 = \kappa_0(1 - \delta)$, the κ_0 is a constant spring constant, and the random number $\delta \in (0, 1)$. We note that throughout the main text the open boundary condition is used since we want to explore the finite noisy systems beyond the traditional periodic Bloch framework. The cases with periodic boundary conditions and perfect unit cells are listed in the Supplemental Material [51].

The calculated projection operator $\hat{P}$ for the different δ will have some different features as shown in Fig. 1(b), which can be captured and learned unsupervisedly by the manifold learning. Following the scheme described above on the dataset $\{\hat{P}_n\}$, we can see that there is a second high value ($j = 1$) in Fig. 1(c), which means that the connections of samples can be reflected by the ϕ_1. If we assign all the samples in the manifold space ϕ_1 and ϕ_2 in Fig. 1(d), we can see obviously the samples could be classified into two different groups according to the δ, with the threshold value $\delta = 0.5$, coinciding with the topological transition of the SSH model. For the SSH chain model, the winding number of this system can be calculated by [59] $v = (1/2\pi i)\int_{-\pi/a}^{\pi/a} dkq^{-1}\partial_k q$, where $q = \kappa_1 + \kappa_2 e^{ika}$, which will be $v = 1$ for $\kappa_1 < \kappa_2$ ($\delta < 0.5$) and $v = 0$ for $\kappa_1 > \kappa_2$ ($\delta > 0.5$).

We introduce random elastic constants in the 1D SSH-like phononic chain, as shown in Fig. 1(e). The calculated eigenvalues λ_j and the manifold space $\{\phi_j\}$ in Figs. 1(f) and 1(g) show that the samples can be also clustered well by our scheme, which resembles the topological transition in the standard SSH phononic model for opposite $\Delta\kappa$. The topologically induced interface states for two disordered

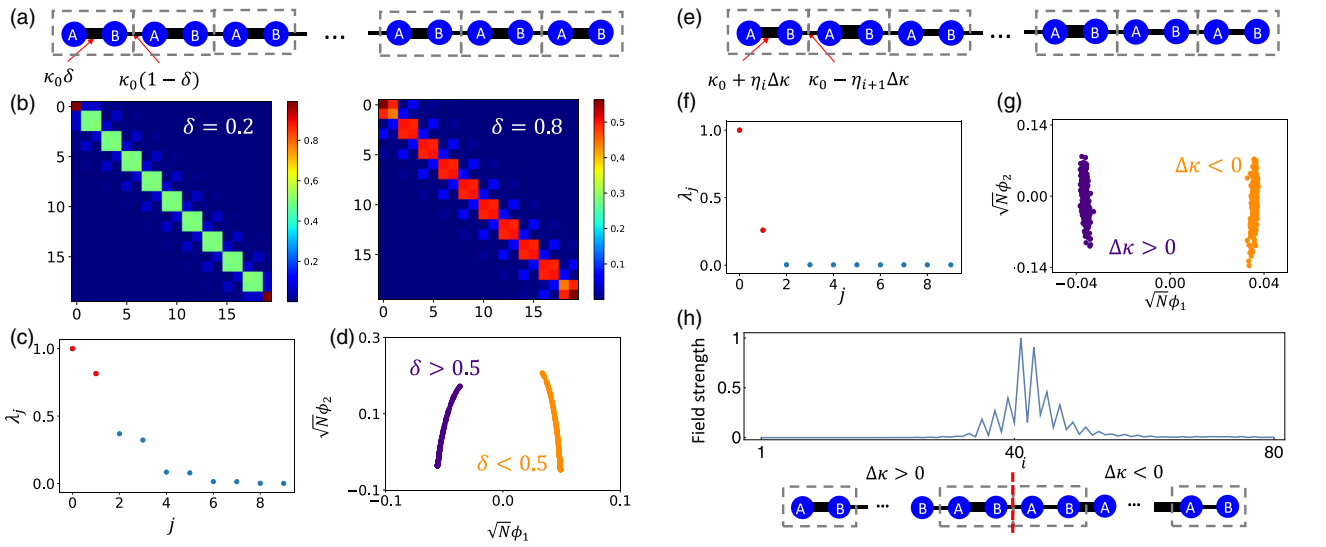

FIG. 1. The unsupervised clustering of 1D phononic SSH model with projection operator $\hat{P}$. (a) The SSH chain with finite size $L = 20$, mass $m = 1.0$, spring constant $\kappa_0 = 1.0$, and $\delta \in (0, 1)$. The gray blocks indicate the unit cells. (b) The projection operator matrix P_{ij} for the cases $\delta = 0.2$ and $\delta = 0.8$. (c) The first ten largest eigenvalues λ_j with $\varepsilon = 0.2$, $N = 1000$, $\omega_c = \sqrt{\kappa_0/m} = 1.0$. (d) Different topological classes are classified unsupervisedly, which coincides with the topological transition ($\delta = 0.5$) in the phononic SSH model. After clustering, we label samples with different colors according to their δ values ($\delta > 0.5$ or $\delta < 0.5$) and confirm the classification. (e) Disordered phononic SSH chain with random elastic constants, where the bias $\Delta\kappa \in (-0.75, 0.75)$ and the spatially dependent random number $\eta_i \in (0, 1)$. (f) The first ten largest eigenvalues λ_j with $\varepsilon = 1.0$, $N = 1000$, $\omega_c = 1.4$. (g) Different topological classes can still be well classified, even if the systems are disordered by noisy couplings. (h) The topological interface mode emerges between two random phononic chains with opposite signs of $\Delta\kappa$ ($\Delta\kappa = 0.72$ and $\Delta\kappa = -0.54$), and $L = 40$. The field strength means the absolute amplitude of displacements (more details in the Supplemental Material [51]).

phononic chains with opposite signs of $\Delta\kappa$ are clearly shown in Fig. 1(h). The successful unsupervised clustering for disordered valley Hall states in 2D honeycomb phononic lattices with random mass biases can be found in the Supplemental Material [51], which is not discernible by the edge modes. Moreover, we would like to note that edge modes can exist for trivial finite structures without nontrivial topology so that, for finite systems with open boundary conditions, the edge modes can be trivial and are nonsufficient to correctly determine topological classes.

Amorphous topological phononics insulators.—Recently, the amorphous phononic lattice from random point sets has shown nontrivial topological properties and robust edge states, which demonstrates that the local interactions and local geometry arrangements are sufficient to generate chiral edge modes [47,48], as shown in Fig. 2. The amorphous phononic topological systems are constructed by gyroscopes that are linked by springs [47], of which the topological properties can be adjusted by the geometric structures and the amorphous types. Because the sample structures are geometrically different due to randomness, we exploit a coarse-grained mapping from the arbitrary amorphous structures into a uniform space for building uniform descriptions, as shown in Fig. 2(a): mapping the average displacement field of oscillators in the dotted block of the real space into the coarse-grained space and then constructing the $\hat{P}^r$ based on the reduced uniform space.

Based on the dataset $\{\hat{P}^r_n\}$, we calculate eigenvalues λ_j associated with the manifold space $\{\phi_j\}$ in Figs. 2(b) and 2(c). We can see the samples can be clustered into three different groups, coinciding with the topological classes of amorphous phononics. For amorphous topological phononics insulators, the local Chern number v is responsible for describing the topological properties [44,47]: $v = 12\pi i \sum_{i\in A}\sum_{j\in B}\sum_{k\in C} P_{ij}P_{jk}P_{ki} - P_{ik}P_{kj}P_{ji}$, where A, B, and C are three areas around the positions (see Supplemental Material [51]). As further demonstrated in Fig. 2(d), two different amorphous phononic topological insulators in samples classified by our scheme indeed show opposite chiral edge modes, with opposite local Chern numbers $v = \pm 1$. The samples in the third group do not show any chiral edge mode, corresponding to the trivial topology with $v = 0$.

Higher-order topological phononics.—Besides these $(d-1)$ topological properties in d-dimension systems, the higher-order topological states ($d-2$ or $d-3$) are attracting much attention [6,7,15,61–63]. Some higher-order topological phononics can be described by the quantized shift of the Wannier center that is related to the Berry connection [6,63]. The higher-order topological phononics can be constructed by the continuum phononic systems and the dynamic equations can be approximately written as $\ddot{x}_i = D_{ij}x_j$ around the resonant frequency ω_0 [15,64], where D_{ij} is the effective coupling between the oscillators x_i and x_j.

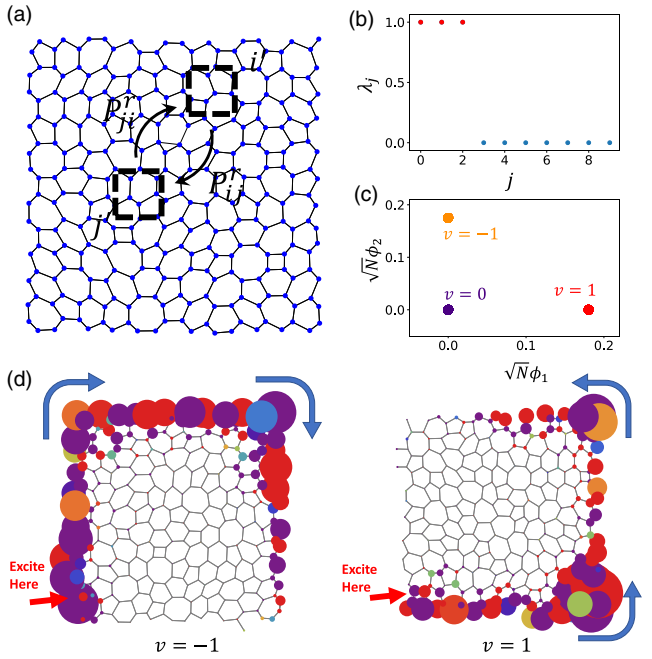

FIG. 2. The unsupervised learning of amorphous topological phononics. (a) The demonstration of the amorphous structure, constructed by connecting adjacent centroids of Delaunay triangulation mesh [60]. The system has size $L = 130 \sim 150$. The projection operator is constructed in the coarse-grained space by averaging displacement field of oscillators in the dotted block of the original space. The reduced dimension is $L_r = 10 \times 10 = 100$. (b) The first ten largest eigenvalues λ_j with $\varepsilon = 0.2$, $N = 300$, $\omega_c = 1.0$. (c) Different classes that are classified unsupervisedly can coincide with different local Chern numbers v. The numbers of samples for $v = (0, -1, 1)$ are 107, 93, 100, respectively. (d) The chiral edge modes in amorphous topological phononics with different local Chern number $v = \pm 1$. The amplitude and phase of phononic field are represented by the radius and colors (from blue to red) of the disks.

The unsupervised learning of the quadrupole higher-order topological insulator (HOTI) is demonstrated in Fig. 3(a). From the eigenvalues λ_j associated with the manifold space $\{\phi_j\}$ in Figs. 3(b) and 3(c), we can see that the N samples can be classified unsupervisedly by the threshold value $\delta = 0.67$. This value deviates from the theoretical one $\delta = 0.5$ predicted in Bloch-momentum space analysis [15,61], due to the finite size effect. As shown in Fig. 3(d), for the finite system, the topological transition point δ, where the corner states emerge and the frequencies become degenerate at the resonant frequency (ω_0, as the effective zero energy), will shift from theoretical value 0.5 to 0.67. This is because the "corner" states, although they decay spatially, will interact with each other when the system size is finite. A perfect phase transition requires a clear separation of those corner states, which will be achieved with further increase of δ to 0.67. This finite size effect of HOTI classification has not been found before in the Bloch picture for periodic infinite systems. The

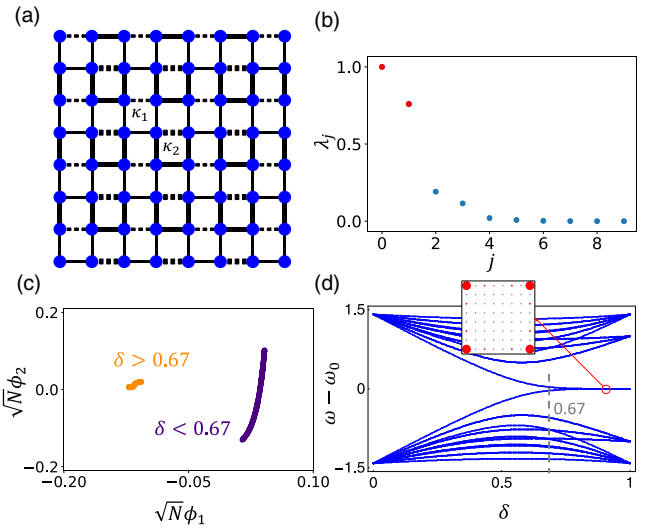

FIG. 3. The unsupervised clustering of higher-order topological phononics. (a) The quadrupole higher-order topological models with coupling strength $\kappa_1 = \kappa_0(1-\delta)$ and $\kappa_2 = \kappa_0\delta$, $\delta \in (0, 1)$. The dotted line means the negative counterpart. $L = 8 \times 8 = 64$. (b) The first ten largest eigenvalues λ_j with $\varepsilon = 1.0$, $N = 500$, $\omega_c = \omega_0$. (c) The structures are well classified into topological classes, corresponding to different value groups of δ. (d) The energy levels as a function of δ show that the unsupervised learning can predict the higher-order topological transition, even at finite size. (Inset) Quadrupole corner states of the higher-order topological phononics.

unsupervised learning for HOTI in phononic kagome lattices can be found in the Supplemental Material [51].

Non-Hermitian topological phononics.—The topological properties in non-Hermitian systems without time-reversal symmetry are very important [65–75]. The non-Hermitian feature can originate from many aspects [76], such as nonreciprocal coupling [77], nonzero dissipation bias, or complex on-site potentials [68,78]. Mathematically, the non-Hermitian system will have complex eigenfrequencies and nonorthogonal eigenvectors [79]. Some Bloch analyses have been applied for non-Hermitian systems and found that the exception points play important roles for the topological origin [68,75,80]. However, the non-Bloch analysis also states the non-Hermitian skin (surface) effect and describes the edge modes as well [70–73]. Thus, the non-Hermitian topological invariants are not clear, in general, and are still under exploration [70–75,80,81].

Here, we consider the 1D phononic lattice with different and random dissipation terms due to the nonzero viscosity $\tau_{A/B} \neq 0$, shown in Fig. 4(a). The dynamic equation can be written as

$$m\frac{\partial^2}{\partial t^2}a_i + \tau_A^i\frac{\partial}{\partial t}a_i = -\kappa(a_i - b_{i-1}) + \kappa(b_i - a_i),$$
$$m\frac{\partial^2}{\partial t^2}b_i + \tau_B^{i+1}\frac{\partial}{\partial t}b_i = -\kappa(b_i - a_i) + \kappa(a_{i+1} - b_i), \qquad (4)$$

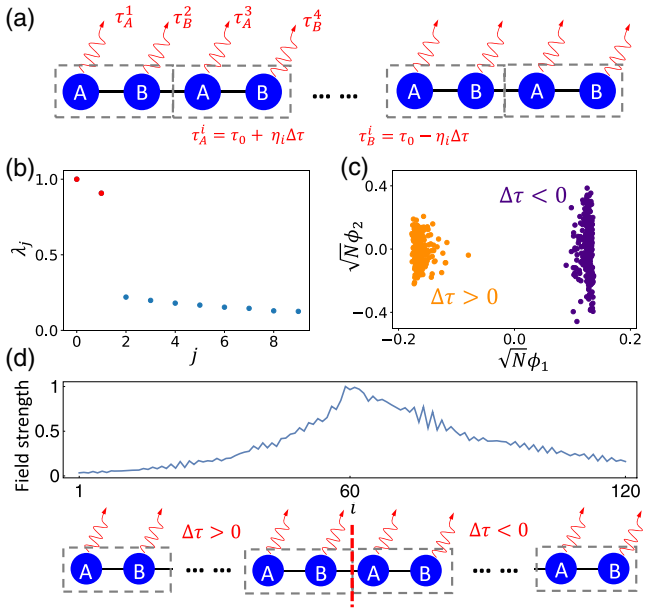

FIG. 4. The unsupervised clustering of 1D non-Hermitian phononic chain. (a) The A/B oscillators have random dissipation losses, with alternatively large and small dissipation values $\tau_{A/B}^i = \tau_0 \pm \eta_i \Delta\tau$, respectively. The length size $L = 20$, the mass $m = 1.0$, the viscosity $\tau_0 = 1.0$, the viscosity bias $\Delta\tau \in (-0.5, 0.5)$, and the random number $\eta_i \in (0, 1)$. (b) The first ten largest eigenvalues λ_j with $\varepsilon = 1.0$, $N = 500$, $\omega_c = 1.35$. (c) Different classes are classified unsupervisedly, which coincides with the fact that the cases of $\tau_A > \tau_B$ ($\Delta\tau > 0$) and $\tau_A < \tau_B$ ($\Delta\tau < 0$) are topologically distinct. (d) The topological interface mode emerges between two non-Hermitian random phononic chains with opposite signs of $\Delta\tau$ ($\Delta\tau = 0.4$ and $\Delta\tau = -0.24$), and $L = 60$.

where $\tau_{A/B}^i$ is the different and random dissipation viscosity terms of A/B oscillators for the different ith oscillator. From the eigenvalues λ_j associated with the manifold space $\{\phi_j\}$ in Figs. 4(b) and 4(c), we can see the N samples are clustered into two different groups: $\Delta\tau > 0$ or $\Delta\tau < 0$ corresponding to the case $\tau_A > \tau_B$ or $\tau_A < \tau_B$, which coincides with the fact that the cases of $\tau_A > \tau_B$ and $\tau_A < \tau_B$ are topologically distinct. As a result, the topological interface state emerges at the interface between two topologically different random non-Hermitian chains with opposite signs of $\Delta\tau$, as shown in Fig. 4(d).

To summarize, we have demonstrated the unsupervised manifold clustering of topological phononics including spatial randomness, amorphous nonperiodic structures, and non-Hermitian dissipations. With real-space representations and their similarity definitions in Eqs. (1) and (2), one can classify diverse topological phononic systems within a single unified scheme without *a priori* knowledge about topological families or defining topological invariants *ad hoc*. Unsupervised manifold learning has achieved efficient nonlinear dimension reductions, which would map the phononic systems into the manifold space based on their features in the real space and then cluster them into different groups associated with different topological properties. Our work would be used to explore diverse topological phononics before defining or introducing topological invariants, which is meaningful for not only theoretical understandings, but also experimental detections [82], especially for the noisy random, non-Hermitian, and out-of-equilibrium open systems and beyond [72–75,80].

We acknowledge the support from the National Key Research Program of China (Grant No. 2016YFA0301101), National Natural Science Foundation of China (No. 11935010, No. 11775159 and No. 61621001), the Shanghai Science and Technology Committee (Grants No. 18ZR1442800 and No. 18JC1410900), and the Opening Project of Shanghai Key Laboratory of Special Artificial Microstructure Materials and Technology.

Note added.—During the review, we became aware of one related preprint [83], studying unsupervised clusterings of topological bands in the momentum space.

*Corresponding author.
Xonics@tongji.edu.cn

[1] Y. Liu, Y. Xu, and W. Duan, Berry phase and topological effects of phonons, Natl. Sci. Rev. **5**, 314 (2017).
[2] S. D. Huber, Topological mechanics, Nat. Phys. **12**, 621 (2016).
[3] L. Zhang, J. Ren, J.-S. Wang, and B. Li, Topological Nature of the Phonon Hall Effect, Phys. Rev. Lett. **105**, 225901 (2010).
[4] G. Ma and P. Sheng, Acoustic metamaterials: From local resonances to broad horizons, Sci. Adv. **2**, e1501595 (2016).
[5] H. Ge, M. Yang, C. Ma, M.-H. Lu, Y.-F. Chen, N. Fang, and P. Sheng, Breaking the barriers: Advances in acoustic functional materials, Natl. Sci. Rev. **5**, 159 (2017).
[6] H. Xue, Y. Yang, F. Gao, Y. Chong, and B. Zhang, Acoustic higher-order topological insulator on a kagome lattice, Nat. Mater. **18**, 108 (2019).
[7] X. Zhang, H.-X. Wang, Z.-K. Lin, Y. Tian, B. Xie, M.-H. Lu, Y.-F. Chen, and J.-H. Jiang, Second-order topology and multidimensional topological transitions in sonic crystals, Nat. Phys. **15**, 582 (2019).
[8] M. Z. Hasan and C. L. Kane, Colloquium: Topological insulators, Rev. Mod. Phys. **82**, 3045 (2010).
[9] D. Xiao, M.-C. Chang, and Q. Niu, Berry phase effects on electronic properties, Rev. Mod. Phys. **82**, 1959 (2010).
[10] A. Bansil, H. Lin, and T. Das, Colloquium: Topological band theory, Rev. Mod. Phys. **88**, 021004 (2016).
[11] R. Süsstrunk and S. D. Huber, Observation of phononic helical edge states in a mechanical topological insulator, Science **349**, 47 (2015).
[12] P. Wang, L. Lu, and K. Bertoldi, Topological Phononic Crystals with One-Way Elastic Edge Waves, Phys. Rev. Lett. **115**, 104302 (2015).

[13] M. Yan, J. Lu, F. Li, W. Deng, X. Huang, J. Ma, and Z. Liu, On-chip valley topological materials for elastic wave manipulation, Nat. Mater. **17**, 993 (2018).

[14] M. Xiao, W.-J. Chen, W.-Y. He, and C. T. Chan, Synthetic gauge flux and Weyl points in acoustic systems, Nat. Phys. **11**, 920 (2015).

[15] M. Serra-Garcia, V. Peri, R. Süsstrunk, O. R. Bilal, T. Larsen, L. Guillermo Villanueva, and S. D. Huber, Observation of a phononic quadrupole topological insulator, Nature (London) **555**, 342 (2018).

[16] Y. Liu, C.-S. Lian, Y. Li, Y. Xu, and W. Duan, Pseudospins and Topological Effects of Phonons in a Kekulé Lattice, Phys. Rev. Lett. **119**, 255901 (2017).

[17] S. H. Mousavi, A. B. Khanikaev, and Z. Wang, Topologically protected elastic waves in phononic metamaterials, Nat. Commun. **6**, 8682 (2015).

[18] C. He, X. Ni, H. Ge, X.-C. Sun, Y.-B. Chen, M.-H. Lu, X.-P. Liu, and Y.-F. Chen, Acoustic topological insulator and robust one-way sound transport, Nat. Phys. **12**, 1124 (2016).

[19] H. He, C. Qiu, L. Ye, X. Cai, X. Fan, M. Ke, F. Zhang, and Z. Liu, Topological negative refraction of surface acoustic waves in a Weyl phononic crystal, Nature (London) **560**, 61 (2018).

[20] P. Zhang, H. Shen, and H. Zhai, Machine Learning Topological Invariants with Neural Networks, Phys. Rev. Lett. **120**,066401 (2018).

[21] J. Venderley, V. Khemani, and E.-A. Kim, Machine Learning Out-of-Equilibrium Phases of Matter, Phys. Rev. Lett. **120**, 257204 (2018).

[22] J. Peurifoy, Y. Shen, L. Jing, Y. Yang, F. Cano-Renteria, B. G. DeLacy, J. D. Joannopoulos, M. Tegmark, and M. Soljačić, Nanophotonic particle simulation and inverse design using artificial neural networks, Sci. Adv. **4**, eaar4206 (2018).

[23] P. Mehta, M. Bukov, C.-H. Wang, A. G. R. Day, C. Richardson, C. K. Fisher, and D. J. Schwab, A high-bias, low-variance introduction to machine learning for physicists, Phys. Rep. **810**, 1 (2019).

[24] V. Dunjko and H. J Briegel, Machine learning & artificial intelligence in the quantum domain: A review of recent progress, Rep. Prog. Phys. **81**, 074001 (2018).

[25] G. Carleo, I. Cirac, K. Cranmer, L. Daudet, M. Schuld, N. Tishby, L. Vogt-Maranto, and L. Zdeborová, Machine learning and the physical sciences, Rev. Mod. Phys. **91**, 045002 (2019).

[26] J. Carrasquilla and R. G. Melko, Machine learning phases of matter, Nat. Phys. **13**, 431 (2017).

[27] Y. Zhang and E.-A. Kim, Quantum Loop Topography for Machine Learning, Phys. Rev. Lett. **118**, 216401 (2017).

[28] E. P. L. Van Nieuwenburg, Y.-H. Liu, and S. D. Huber, Learning phase transitions by confusion, Nat. Phys. **13**, 435 (2017).

[29] G. Carleo and M. Troyer, Solving the quantum many-body problem with artificial neural networks, Science **355**, 602 (2017).

[30] L. Pilozzi, F. A. Farrelly, G. Marcucci, and C. Conti, Machine learning inverse problem for topological photonics, Commun. Phys. **1**, 57 (2018).

[31] Y. Long, J. Ren, Y. Li, and H. Chen, Inverse design of photonic topological state via machine learning, Appl. Phys. Lett. **114**, 181105 (2019).

[32] D. Liu, Y. Tan, E. Khoram, and Z. Yu, Training deep neural networks for the inverse design of nanophotonic structures, ACS Photonics **5**, 1365 (2018).

[33] W. Ma, F. Cheng, and Y. Liu, Deep-learning-enabled on-demand design of chiral metamaterials, ACS Nano **12**, 6326 (2018).

[34] Z. Liu, D. Zhu, S. P. Rodrigues, K.-T. Lee, and W. Cai, Generative model for the inverse design of metasurfaces, Nano Lett. **18**, 6570 (2018).

[35] L. Wang, Discovering phase transitions with unsupervised learning, Phys. Rev. B **94**, 195105 (2016).

[36] S. J. Wetzel, Unsupervised learning of phase transitions: From principal component analysis to variational autoencoders, Phys. Rev. E **96**, 022140 (2017).

[37] J. F. Rodriguez-Nieva and M .S. Scheurer, Identifying topological order through unsupervised machine learning, Nat. Phys. **15**, 790 (2019).

[38] A. Andreassen, I. Feige, C. Frye, and M. D. Schwartz, Junipr: A framework for unsupervised machine learning in particle physics, Eur. Phys. J. C **79**, 102 (2019).

[39] P. Baldi, P. Sadowski, and D. Whiteson, Searching for exotic particles in high-energy physics with deep learning, Nat. Commun. **5**, 4308 (2014).

[40] V. Tshitoyan, J. Dagdelen, L. Weston, A. Dunn, Z. Rong, O. Kononova, K. A. Persson, G. Ceder, and A. Jain, Unsupervised word embeddings capture latent knowledge from materials science literature, Nature (London) **571**, 95 (2019).

[41] N. Marzari, A. A. Mostofi, J. R. Yates, I. Souza, and D. Vanderbilt, Maximally localized Wannier functions: Theory and applications, Rev. Mod. Phys. **84**, 1419 (2012).

[42] A. A. Soluyanov and D. Vanderbilt, Wannier representation of $\mathbb{Z}_2$ topological insulators, Phys. Rev. B **83**, 035108 (2011).

[43] R. Bianco and R. Resta, Mapping topological order in coordinate space, Phys. Rev. B **84**, 241106(R) (2011).

[44] A. Kitaev, Anyons in an exactly solved model and beyond, Ann. Phys. (N.Y.) **321**, 2 (2006).

[45] J. B. Tenenbaum, V. De Silva, and J. C. Langford, A global geometric framework for nonlinear dimensionality reduction, Science **290**, 2319 (2000).

[46] S. T. Roweis and L. K. Saul, Nonlinear dimensionality reduction by locally linear embedding, Science **290**, 2323 (2000).

[47] N. P. Mitchell, L. M. Nash, D. aniel Hexner, A. M. Turner, and W. T. M. Irvine, Amorphous topological insulators constructed from random point sets, Nat. Phys. **14**, 380 (2018).

[48] A. Agarwala and V. B. Shenoy, Topological Insulators in Amorphous Systems, Phys. Rev. Lett. **118**, 236402 (2017).

[49] R. R. Coifman and S. Lafon, Diffusion maps, Appl. Comput. Harmon. Anal. **21**, 5 (2006).

[50] R. R. Coifman, S. Lafon, A. B. Lee, M. Maggioni, B. Nadler, F. Warner, and S. W. Zucker, Geometric diffusions as a tool for harmonic analysis and structure definition of data: Diffusion maps, Proc. Natl. Acad. Sci. U.S.A. **102**, 7426 (2005).

[51] See Supplemental Material at http://link.aps.org/supplemental/10.1103/PhysRevLett.124.185501 for details about topological valley phononics, HOTI in phononic kagome lattices, the equations of motions, effects from experimental noisy data, and unsupervised learning of topological phononics based on the features in momentum space, which includes Refs. [52–58].
[52] M. Bernstein and L. S. Brown, Supersymmetry and the Bistable Fokker-Planck Equation, Phys. Rev. Lett. **52**, 1933 (1984).
[53] J. Lu, C. Qiu, L. Ye, X. Fan, M. Ke, F. Zhang, and Z. Liu, Observation of topological valley transport of sound in sonic crystals, Nat. Phys. **13**, 369 (2017).
[54] A. Raman and S. Fan, Photonic Band Structure of Dispersive Metamaterials Formulated as a Hermitian Eigenvalue Problem, Phys. Rev. Lett. **104**, 087401 (2010).
[55] S. Petitgrand, R. Yahiaoui, K. Danaie, A. Bosseboeuf, and J. P. Gilles, 3D measurement of micromechanical devices vibration mode shapes with a stroboscopic interferometric microscope, Opt. Lasers Eng. **36**, 77 (2001).
[56] R. Givens, O. F. de Alcantara Bonfim, and R. B Ormond, Direct observation of normal modes in coupled oscillators, Am. J. Phys **71**, 87 (2003).
[57] P. J. Georgas and G. S. Schajer, Simultaneous measurement of plate natural frequencies and vibration mode shapes using espi, Exp. Mech. **53**, 1461 (2013).
[58] C.-H. Huang and C.-C. Ma, Experimental measurement of mode shapes and frequencies for vibration of plates by optical interferometry method, J. Vib. Acoust. **123**, 276 (2001).
[59] R. Süsstrunk and S. D. Huber, Classification of topological phonons in linear mechanical metamaterials, Proc. Natl. Acad. Sci. U.S.A. **113**, E4767 (2016).
[60] M. Florescu, S. Torquato, and P. J. Steinhardt, Designer disordered materials with large, complete photonic band gaps, Proc. Natl. Acad. Sci. U.S.A. **106**, 20658 (2009).
[61] W. A. Benalcazar, B. A. Bernevig, and T. L. Hughes, Quantized electric multipole insulators, Science **357**, 61 (2017).
[62] X. Zhang, B.-Y. Xie, H.-F. Wang, X. Xu, Y. Tian, J.-H. Jiang, M.-H. Lu, and Y.-F. Chen, Dimensional hierarchy of higher-order topology in three-dimensional sonic crystals, Nat. Commun. **10**, 5331 (2019).
[63] X. Ni, M. Weiner, A. Alù, and A. B. Khanikaev, Observation of higher-order topological acoustic states protected by generalized chiral symmetry, Nat. Mater. **18**, 113 (2019).
[64] K. H. Matlack, M. Serra-Garcia, A. Palermo, S. D Huber, and C. Daraio, Designing perturbative metamaterials from discrete models, Nat. Mater. **17**, 323 (2018).
[65] S. Diehl, E. Rico, M. A Baranov, and P. Zoller, Topology by dissipation in atomic quantum wires, Nat. Phys. **7**, 971 (2011).
[66] K. Ding, G. Ma, M. Xiao, Z. Q. Zhang, and C. T. Chan, Emergence, Coalescence, and Topological Properties of Multiple Exceptional Points and Their Experimental Realization, Phys. Rev. X **6**, 021007 (2016).
[67] J. M. Zeuner, M. C Rechtsman, Y. Plotnik, Y. Lumer, S. Nolte, M. S. Rudner, M. Segev, and A. Szameit, Observation of a Topological Transition in the Bulk of a Non-Hermitian System, Phys. Rev. Lett. **115**, 040402 (2015).
[68] D. Leykam, K. Y. Bliokh, C. Huang, Y. D. Chong, and F. Nori, E. Modes, Degeneracies, and Topological Numbers in Non-Hermitian Systems, Phys. Rev. Lett. **118**, 040401 (2017).
[69] K. Ding, G. Ma, Z. Q. Zhang, and C. T. Chan, Experimental Demonstration of an Anisotropic Exceptional Point, Phys. Rev. Lett. **121**, 085702 (2018).
[70] V. M. M. Alvarez, J. E. B. Vargas, and L. E. F. F. Torres, Non-hermitian robust edge states in one dimension: Anomalous localization and eigenspace condensation at exceptional points, Phys. Rev. B **97**, 121401(R) (2018).
[71] F. K. Kunst, E. Edvardsson, J. C. Budich, and E. J. Bergholtz, Biorthogonal Bulk-Boundary Correspondence in Non-Hermitian Systems, Phys. Rev. Lett. **121**, 026808 (2018).
[72] H. Shen, B. Zhen, and L. Fu, Topological Band Theory for Non-Hermitian Hamiltonians, Phys. Rev. Lett. **120**, 146402 (2018).
[73] S. Yao and Z. Wang, Edge States and Topological Invariants of Non-Hermitian Systems, Phys. Rev. Lett. **121**, 086803 (2018).
[74] K. Dasbiswas, K. K Mandadapu, and S. Vaikuntanathan, Topological localization in out-of-equilibrium dissipative systems, Proc. Natl. Acad. Sci. U.S.A. **115**, E9031 (2018).
[75] Z. Gong, Y. Ashida, K. Kawabata, K. Takasan, S. Higashikawa, and M. Ueda, Topological Phases of Non-Hermitian Systems, Phys. Rev. X **8**, 031079 (2018).
[76] A. Ghatak and T. Das, New topological invariants in non-hermitian systems, J. Phys. Condens. Matter **31**, 263001 (2019).
[77] T. E. Lee, Anomalous Edge State in a Non-Hermitian Lattice, Phys. Rev. Lett. **116**, 133903 (2016).
[78] M. Wang, L. Ye, J. Christensen, and Z. Liu, Valley Physics in Non-Hermitian Artificial Acoustic Boron Nitride, Phys. Rev. Lett. **120**, 246601 (2018).
[79] C. M. Bender, Making sense of non-Hermitian Hamiltonians, Rep. Prog. Phys. **70**, 947 (2007).
[80] E. J. Bergholtz, J. Carl Budich, and F. K. Kunst, Exceptional topology of non-Hermitian systems, arXiv:1912.10048.
[81] T. Liu, Y.-R. Zhang, Q. Ai, Z. Gong, K. Kawabata, M. Ueda, and F. Nori, Second-Order Topological Phases in Non-Hermitian Systems, Phys. Rev. Lett. **122**, 076801 (2019).
[82] J. Ren, W.-X. Wang, B. Li, and Y.-C. Lai, Noise Bridges Dynamical Correlation and Topology in Coupled Oscillator Networks, Phys. Rev. Lett. **104**, 058701 (2010).
[83] M. S. Scheurer and R.-J. Slager, Unsupervised machine learning and band topology, arXiv:2001.01711.